Experimental and molecular modeling studies on the interaction of the Ru(II)–piroxicam with DNA and BSA

ARTICLE *in* EUROPEAN JOURNAL OF MEDICINAL CHEMISTRY · SEPTEMBER 2013

Impact Factor: 3.45 · DOI: 10.1016/j.ejmech.2013.08.051 · Source: PubMed

5 AUTHORS, INCLUDING:

Taghi Khayamian
Isfahan University of Technology
107 PUBLICATIONS **1,562** CITATIONS
SEE PROFILE

Hadi Amiri Rudbari
University of Isfahan
161 PUBLICATIONS **518** CITATIONS
SEE PROFILE

European Journal of Medicinal Chemistry 69 (2013) 577–590

Contents lists available at ScienceDirect

European Journal of Medicinal Chemistry

journal homepage: http://www.elsevier.com/locate/ejmech

Original article

Experimental and molecular modeling studies on the interaction of the Ru(II)-piroxicam with DNA and BSA

Zahra Jannesari [a], Hassan Hadadzadeh [a,*], Taghi Khayamian [a], Batool Maleki [a], Hadi Amiri Rudbari [b]

[a] Department of Chemistry, Isfahan University of Technology, Isfahan 84156-83111, Iran
[b] Faculty of Chemistry, University of Isfahan, Isfahan 81746-73441, Iran

ARTICLE INFO

Article history:
Received 21 June 2013
Received in revised form
26 August 2013
Accepted 31 August 2013
Available online 15 September 2013

Keywords:
Ru(II) complex
DNA binding
Fluorescence quenching
Bovine serum albumin
Molecular modeling
Photocleavage

ABSTRACT

A mononuclear Ru(II) complex containing two piroxicam (Pir^-) ligands was synthesized and fully characterized. Interaction studies of the Pir^- anion and the Ru(II) complex with DNA and BSA were carried out using spectroscopic techniques. The results suggested that the Pir^- anion binds to DNA in a moderately strong fashion via intercalation between the base stacks of double–stranded DNA, while the Ru(II) complex is a groove binder and interacts with DNA with more affinity. Moreover, the results demonstrated that the microenvironment and the secondary structure of BSA were changed in the presence of Pir^- and Ru(II) complex. The free Pir^- ligand and the Ru(II) complex can lead to the photocleavage of DNA supercoiled pUC57. Finally, the binding of the Ru(II) complex to BSA and DNA was modeled by molecular docking and molecular dynamic simulation methods.

1. Introduction

Since the discovery of antitumor and anti-metastatic properties of cisplatin, intensive studies have been performed on cytotoxic compounds with more acceptable toxicity profiles because the clinical applications of cisplatin and its analogs are hindered by some major problems such as drug resistance and systemic toxicity [1]. These important problems in platinum based anticancer drugs have stimulated more research efforts to investigate drugs based on other transition metals [2]. Among the different metal complexes generating interests, ruthenium complexes are the best candidates, because several oxidation states are accessible for ruthenium under physiological condition and its complexes can mimic iron in binding to albumin and transferrin with lower toxicity than that of platinum therapies [3]. The biological activity of ruthenium compounds was first recognized in the 1950s and their anticancer activity was reported in the 1960s [4,5]. Although many ruthenium compounds show significant efficacy and lower toxicity against various types of tumors than the Pt(II)-based drugs but two Ru-based drugs, NAMI-A {(ImH)[*trans*-$RuCl_4$(DMSO)(Im)] (Im = imidazole)}, and KP1019 {(IndH)[*trans*-$RuCl_4(Ind)_2$]) (Ind = indazole)} are the only ruthenium drugs that have entered clinical trials [6]. NAMI-A is effective against lung metastases and KP1019 is active against colon carcinomas [7,8]. Though the antitumor mechanism of ruthenium compounds has not been exactly identified, several factors are thought to be responsible for their pharmacological activity. Aquation is an important accepted step for the act of such species. In details, they are rapidly hydrolyzed *in vivo* forming a number of potentially active species, which can facilitate their binding with biomolecules and the rate of this process can strongly affect their antitumor activities [9–11]. More than aquation, the *in vivo* reduction of Ru(III) to Ru(II) and the ability of ruthenium to accumulate specifically in cancer tissues, are also thought to be important for their mechanism of action [9,12]. Moreover, hydrophobic interactions have shown to be very important in the biological activities of some ruthenium anticancer agents [13]. In details, DNA binding seems to play an important role for Ru(II)–arene complexes, which can interact with DNA by direct coordination to the bases, intercalation and stereospecific H-bonding, while other targets such as plasma proteins and glutathione are thought to be more important in the action of Ru(III) complexes [14].

Considering the ruthenium fundamental importance, investigations on ruthenium complexes of pharmaceutical compounds

* Corresponding author. Tel.: +98 311 3913240; fax: +98 311 3912350.
E-mail addresses: hadad@cc.iut.ac.ir, hadadzadeh1347@yahoo.com (H. Hadadzadeh).

0223-5234/$ – see front matter © 2013 Elsevier Masson SAS. All rights reserved.
http://dx.doi.org/10.1016/j.ejmech.2013.08.051

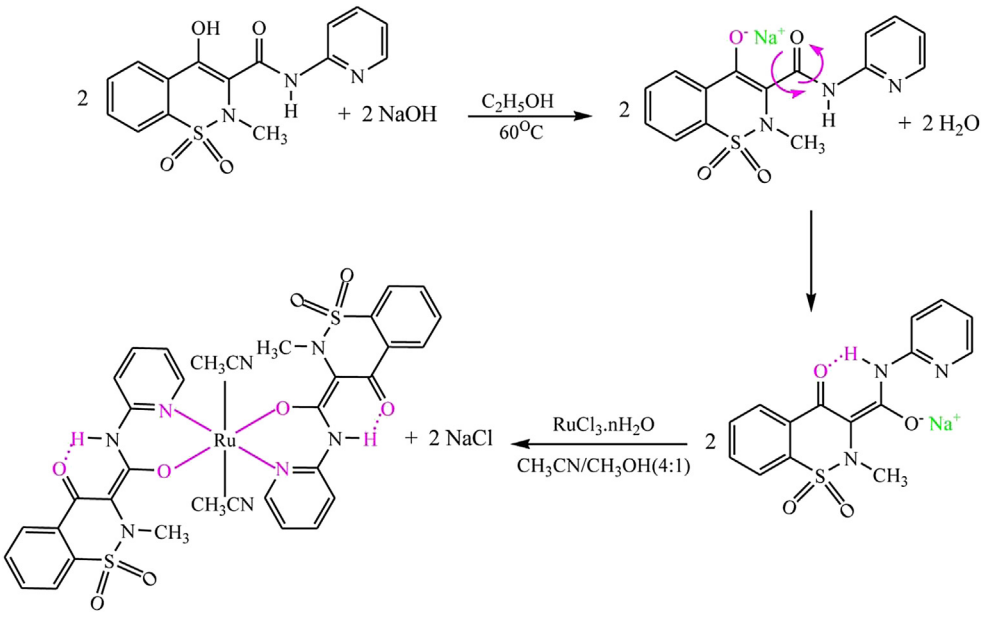

Scheme 1. Synthesis route of *trans*-[Ru(Pir)$_2$(CH$_3$CN)$_2$].

towards DNA and protein are of current interest in connection with information about drug design and tools of molecular biology. Piroxicam is currently the most widely used oxicam which exhibits chemopreventive and chemosuppressive effects in different kinds of cancer such as colon, lung and breast cancer [15]. Due to pharmacological applications of Ru(II) complexes, this article reports the synthesis, spectral characterization, DNA and BSA binding and photocleavage properties of a new mononuclear Ru(II) complex with piroxicam, *trans*-[Ru(Pir)$_2$(CH$_3$CN)$_2$]. The coordination of the piroxicam anion to the Ru(II) ion can provide an enhanced activity of the drug because of the synergism between the ligand and metal properties. In addition, the interactions of the Ru(II) complex with DNA and BSA were modeled by molecular docking and molecular dynamic simulation methods.

2. Experimental section

2.1. Materials

Piroxicam (4-hydroxy-2-methyl-N-2-pyridyl-2H-1,2-benzothiazine-3-carboxamide-1,1-dioxide, Pir) was a gift from the Darou Pakhsh Pharmaceutical Company. Analytical grade $RuCl_3 \cdot 3H_2O$ was purchased from Merck. All solvents were high purity Merck compounds and used without any further purification. Double-stranded fish sperm deoxyribonucleic acid (ds–FS–DNA), bovine serum albumin (BSA) and agarose (molecular biology grade) were purchased from Sigma–Aldrich. Tris(hydroxymethyl)-aminomethane (Tris) buffer and ethidium bromide (3,8-diamino-5-ethyl-6-phenylphenanthridinium bromide, EthBr) were of analytical reagent grade and obtained from Merck. The plasmid pUC57 DNA was isolated from *E. coli* strain by standard procedures and dissolved in TBE buffer (4.5×10^{-2} M Tris, 4.5×10^{-2} M H_3BO_3, and 10^{-3} M EDTA, pH = 8.3).

2.2. Apparatus

Elemental analysis was performed using a Heraeus CHN–O-Rapid elemental analyzer. Fourier transform infrared spectra were recorded on an FT-IR JASCO 680-PLUS spectrometer in the region of 4000–400 cm^{-1} using KBr pellets. Electronic spectra were obtained using a UV-JASCO-570 spectrometer. NMR spectra were recorded on a Bruker DRX-500 MHz Avance spectrometer at ambient temperature in DMSO-d$_6$ with tetramethylsilane (TMS; $\delta = 0$ ppm) as internal standard. Fluorescence measurements were carried out on a Perkin–Elmer LS55 fluorescence spectrometer, using a quartz cell of 1 cm path length.

2.3. Synthesis of trans-[Ru(Pir)$_2$(CH$_3$CN)$_2$]

An ethanolic solution (8 mL) of NaOH (0.3 mmol, 12.0 mg) was added dropwise with stirring to a solution of piroxicam (0.3 mmol, 199 mg) in ethanol (8 mL) in a 1:1 M ratio. The ethanol was removed through evaporation during the crystallization of mono-anionic piroxicam (Pir$^-$). The yellow microcrystalline powder, Na$^+$Pir–, was dissolved in acetonitrile, and to this yellow solution, an acetonitrile/methanol (4:1) solution of $RuCl_3 \cdot 3H_2O$ (0.15 mmol, 39.2 mg) was added. The reaction mixture was stirred and refluxed under a nitrogen atmosphere for 7 h (Scheme 1). The solution was slowly evaporated to dryness at room temperature to yield a reddish-brown solid which was purified by chromatography over silica gel 60 (0.063–0.100 mm) using acetonitrile/toluene (2:1, v/v) as an eluent. The brown band was collected and filtered to remove any solid impurities. After 1 week at room temperature, reddish-brown single crystals of *trans*-[Ru(Pir)$_2$(CH$_3$CN)$_2$] suitable for X-ray analysis were formed by slow evaporation of an acetonitrile/toluene solution in a yield of 71%. Anal. Calc. for $C_{34}H_{30}RuN_8O_8S_2$ (MW = 843.85): C, 48.39; H, 3.58; N, 13.28; S, 7.60%. Found: C, 48.63; H, 3.62; N, 13.21; S, 7.68%. IR: ν_{max}, cm^{-1}; ν(C=O)$_{amide}$, 1622.8; ν(C=N)$_{pyr}$, 1571.7; $\nu_{asym}(SO_2)$, 1352; $\nu_{sym}(SO_2)$, 1182 (KBr disk); UV–Vis: λ, nm (ε, M^{-1} cm^{-1}) in acetonitrile: 378 (21800), 246 (24640); ^{1}H NMR (DMSO-d$_6$): δ, ppm; 2.548 (s, 6H), 2.808 (s, 6H), 7.148 (t, 2H), 7.74 (m, 8H), 7.891 (t, 2H), 8.089 (d, 2H), 8.565 (d, 2H), 15.13 (s, 2H) (See Supplementary information for the ^{1}H and ^{13}C NMR spectra of Pir$^-$ and *trans*-[Ru(Pir)$_2$(CH$_3$CN)$_2$]).

2.4. X-ray crystallographic procedure

The crystal structure of *trans*-[Ru(Pir)$_2$(CH$_3$CN)$_2$] was obtained by the single crystal X-ray diffraction technique. Reddish-brown single crystals of the complex were grown by the slow

Table 1
Crystallographic and structure refinement data for *trans*-[Ru(Pir)$_2$(CH$_3$CN)$_2$].

Empirical formula	C_{34} H_{30} N_8 O_8 Ru S_2
Formula Weigh	843.85
T (K)	293 (2)
λ (Å)	0.71073
Crystal system	Triclinic
Space group	*P-1*
a (Å)	8.2461(2)
b (Å)	8.7492(2)
c (Å)	12.7671(3)
α (°)	82.8600(10)
β (°)	81.8070(10)
γ (°)	85.4050(10)
V (Å^3)	902.81(4)
Z	1
D_x (Mg m^{-3})	1.552
θ range for data collection (°)	2.7–26.0
F (000)	430
Index ranges	$-10 \le h \le 10$ $-10 \le k \le 10$ $-15 \le l \le 15$
Number of measured reflections	29693
Reflections with $I > 2\sigma(I)$	3378
R_{int}	0.025
Data/restraints/parameters	3533/0/247
Goodness-of-fit on F^2 (S)	1.07
Final R indices	$R_1 = 0.0255$ $wR_2 = 0.0692$
R indices (all data)	$R_1 = 0.0274$ $wR_2 = 0.0716$
Number of independent reflections used for refinement	3533
Largest difference in peak and hole (e Å^{-3})	−0.27, 0.39

evaporation of a 2:1 acetonitrile/toluene solution. X-ray diffraction measurements were performed on a Bruker APEX II CCD area-detector diffractometer using Mo $K\alpha$ radiation (λ = 0.71073 Å) at 293(2) K. Data collection, cell refinement, data reduction and absorption correction were performed using multiscan method with Bruker software [16]. The structure was solved by direct method using SIR2004 [17]. The non-hydrogen atoms were refined anisotropically by the full-matrix least-squares method on F2 using SHELXL [18]. All the hydrogen atoms of the ligands were placed at the calculated positions and constrained to ride on their parent atoms. Details concerning collection and analysis are reported in Table 1 and selected bond lengths and angles of the molecular structure of *trans*-[Ru(Pir)$_2$(CH$_3$CN)$_2$] are gathered in Table 2.

2.5. DNA binding experiments

Doubly distilled deionized water was used to prepare the solutions for DNA interaction studies. All the experiments involving interaction of the Ru(II) complex with ds–FS–DNA were performed in Tris–HCl/NaCl buffer (pH = 7.2). A stock solution of ds–FS–DNA was prepared by dissolving the desired amount of DNA in the Tris–HCl/NaCl buffer solution and then filtering through a Millipore filter. The concentration of ds–FS–DNA per nucleotide was determined using a molar absorptivity of 6600 dm^3 mole^{-1} cm^{-1} at 260 nm after 1:1000 dilutions. The 260/280 ratio of 1.81 indicated that the ds–FS–DNA was sufficiently free of protein Ref. [19]. The DNA stock solution was stored at 4 °C in the dark and used within 4 days after preparation. A stock solution of the Ru(II) complex was prepared by dissolving the complex in an aqueous solution of DMSO as the co-solvent, and then diluted suitably with the corresponding buffer to the required concentrations for all the experiments. The final DMSO concentration never exceeded 0.7% v/v. The spectral features (*i.e.* UV–Vis spectra) of *trans*-[Ru(Pir)$_2$(CH$_3$CN)$_2$] did not change on keeping its buffered solution for 24 h and no precipitation or turbidity was observed even after long storage at room temperature (at least 1 months after preparation), which indicate stability of the Ru(II) complex. The Pir$^-$ solution was papered in the same way. In a typical experiment, 2.5 mL solution of the Ru(II) complex (25.00 μM) in 0.7% DMSO/5 mM Tris–HCl/10 mM NaCl buffer at pH 7.2 was prepared and transferred into a cuvette of 1 cm path length. Absorbance titration was determined by adding a concentrated stock solution of FS-DNA (1.97 × 10^{-2} M) directly to the cuvette at 298 K. UV–Vis spectra were recorded after each addition of DNA solution and the intrinsic binding constant, K_b, for DNA binding to the Ru(II) complex was calculated. Absorbance titration of the Pir$^-$ solution (35.00 μM in 0.7% DMSO/5 mM Tris–HCl/10 mM NaCl buffer, pH = 7.2) was carried out in the same way and the effect of DNA addition on the absorption intensity of the Pir$^-$ solution was measured. The binding specificity of the Pir$^-$ anion as an intercalator was studied by the fluorescence displacement titration method using ethidium bromide (EthBr) as a well-known intercalator [20]. EthBr–DNA solution containing 1.3 × 10^{-6} M DNA and 1.3 × 10^{-4} M EthBr was excited at 520 nm in the absence and presence of different concentrations of the Pir$^-$ anion for the EthBr displacement reaction. The fluorescence spectra were collected in the range of 535–680 nm.

Emission intensity measurements of the Ru(II) complex were carried out by adding increasing amounts of FS-DNA to a fixed concentration solution of the complex (25 μM) contained in a quartz cell, and recording the fluorescence spectra after each addition. The extinction wavelength was fixed at 290 nm and the emission spectra were recorded in the range of 315–435 nm. The excitation and emission slits set at 10 and 8 nm, respectively.

Table 2
Selected bond lengths (Å) and angles (°) for *trans*-[Ru(Pir)$_2$(CH$_3$CN)$_2$].

Bond lengths (Å)			
Ru1–N4i	2.0093 (16)	Ru1–O1i	2.0648(12)
Ru1–N4	2.0093 (16)	Ru1–N3i	2.0793 (15)
Ru1–O1	2.0648 (12)	Ru1–N3	2.0793 (15)
Angles bond (°)			
N4i–Ru1–N4	180.00 (9)	N4–Ru1–N3i	90.80 (6)
N4i–Ru1–O1	89.88 (6)	O1–Ru1–N3i	90.20 (5)
N4–Ru1–O1	90.12 (6)	O1i–Ru1–N3i	89.80 (5)
N4i–Ru1–O1i	90.12 (6)	N4i–Ru1–N3	90.80 (6)
N4–Ru1–O1i	89.88 (6)	N4–Ru1–N3	89.20 (6)
O1–Ru1–O1i	180.00 (5)	O1–Ru1–N3	89.80 (5)
N4i–Ru1–N3i	89.20 (6)	O1i–Ru1–N3	90.20 (5)
N3i–Ru1–N3	180.00 (6)		

2.6. BSA binding experiments

All BSA solutions were prepared in the 5 mM Tris–HCl/10 mM NaCl buffer to keep pH value constant (pH = 7.4). The BSA stock solution was stored at 4 °C in the dark and used within 2 h. The interaction studies of BSA with the Pir$^-$ anion and the Ru(II) complex were performed using absorption titration experiment at room temperature. A 2.5 mL operating solution (6 × 10^{-6} M BSA) was titrated by successive additions of stock solutions of the Pir$^-$ anion and the Ru(II) complex and changes in the BSA absorption were recorded after each addition.

In the tryptophan fluorescence quenching experiment, quenching of the tryptophan residues of BSA was performed by taking a fixed concentration of the BSA solution (6 × 10^{-6} M BSA) with increasing amounts of the Pir$^-$ anion and the Ru(II) complex. The fluorescence spectra were recorded at an excitation wavelength of 290 nm and emission was observed between 308 and 460 nm after each addition of the quencher and results were analyzed.

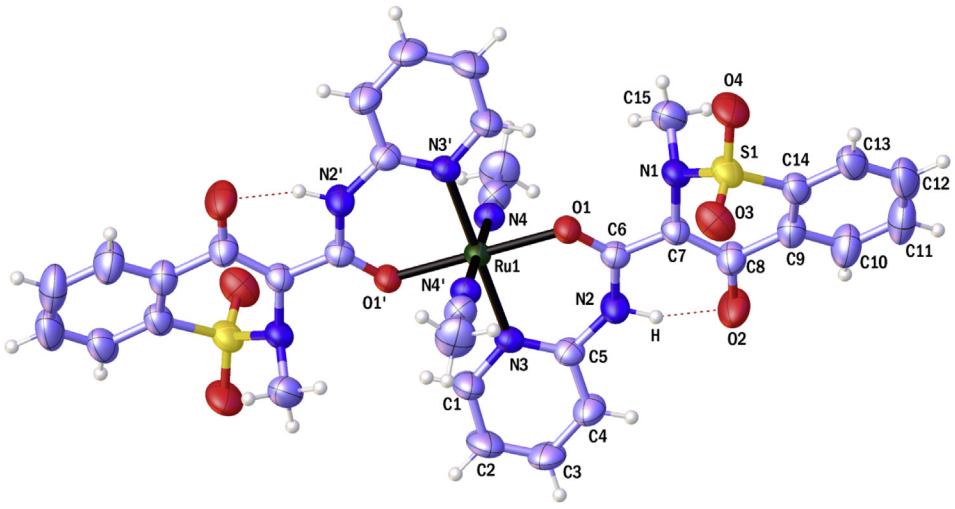

Fig. 1. ORTEP drawing of the *trans*-[Ru(Pir)$_2$(CH$_3$CN)$_2$].

2.7. DNA cleavage activity

The photocleavage of plasmid pUC57 DNA was performed by mean of agarose gel electrophoresis. For the gel electrophoresis experiments, 50 ng pUC57 supercoiled DNA was treated with a different concentration of the Pir$^-$ anion and the Ru(II) complex in Tris–HCl/NaCl buffer and the mixture was incubated at 37 °C for 30 min. After incubation, the samples were irradiated by 360 nm light and electrophoresed for 1 h at 5 V/cm field on a 1% agarose gel containing 10 μg/mL ethidium bromide in TBE buffer (4.5×10^{-2} M Tris + 4.5×10^{-2} M H_3BO_3 + 10^{-3} M EDTA, pH = 8.3). The gel was visualized using a UV transilluminator (UVItec Gel Doc system).

2.8. Molecular modeling and docking

The molecular docking was performed by Autodock 4.2 package using the Lamarckian genetic algorithm (LGA) method [21]. Autodock is a suitable program for an actual docking simulation [22]. Molgero virtual docker (MVD) package was used to produce molecular images and animations [23]. The schematic two-dimensional representations of the docking results were performed using LIGPLOT [24].

2.9. Molecular dynamics (MD) simulations on BSA and DNA

The crystal structure of BSA at a resolution of 2.47 Å (PDB id: 4F5S) and DNA sequence d(ACCGACGTCGGT)$_2$ at a resolution of 1.60 Å (PDB id: 423D) were taken from the protein data bank. The structures of BSA and DNA were simulated in a water box. The MD simulations were performed using the GROMACS 4.5.1 package [25]. The topology parameters of BSA and DNA were created by the GROMOS96 43a1 and Amber99 force field, respectively [26]. The interaction parameters were computed using intermolecular (non-bonded) potential represented as a sum of Lennard–Jones (LJ) force and pairwise Coulomb interaction and the long-range electrostatic force determined by the Particle-Mesh Ewald (PME) method [27,28]. The velocity Verlet algorithm was used for the numerical integrations, and a Maxwellian distribution at the given absolute temperature was used to generate the initial atomic velocities [29]. The BSA and DNA systems were immersed in cubic box ($8.17 \times 8.17 \times 8.17$ nm^3) and ($7.54 \times 7.54 \times 7.54$ nm^3), respectively. The water molecules were added using a simple charge (SPC216) model [30] and the solvated systems were neutralized by adding sixteen Na^+ ions to the BSA system and twenty-two Na^+ ions to the DNA system. Initially, the energy minimization was performed before implementing the position restraint procedure. Then, the full system was subjected to 6000 ps MD at constant pressure (1 bar) and constant temperature (310 K) using the Berendsen thermostat [31]. The MD simulation and results analysis were carried out on the open SUSE 11.3 Linux on an Intel Core 2 Quad Q6600 2.4 GHz and 4 GB of RAM.

The stability of two systems and the structural geometries were examined by means of the root-mean-square deviations (RMSDs) of BSA and DNA with respect to the initial structures of BSA and DNA. The average RMSD values of the BSA and DNA backbones were calculated to be 8.33 nm and 5.50 nm, respectively. The equilibrated conformation of the BSA and DNA were used for docking.

3. Results and discussion

3.1. Synthesis and crystal structure

The mononuclear Ru(II) complex was synthesized in good yield (71%). The air-stable reddish-brown precipitate was purified by chromatography and recrystallized in an acetonitrile/toluene solution to yield *trans*-[Ru(Pir)$_2$(CH$_3$CN)$_2$]. The crystallographic data show that the coordination sphere is pseudo–octahedral and the piroxicam anion acts as a deprotonated bidentate ligand and chelates to the Ru(II) center through the pyridine nitrogen and the amide oxygen at the equatorial positions with a *trans* arrangement (Fig. 1). The apical sites are occupied by the nitrogen atoms of two acetonitrile ligands. Relevant details about the structural refinements are listed in Table 1. The selected bond lengths and angles for *trans*-[Ru(Pir)$_2$(CH$_3$CN)$_2$] are listed in Table 2.

3.2. Spectroscopic studies

IR spectrum of piroxicam is well described and assignment of all bands can be found elsewhere [32]. Upon complexation, the shift of ν(C=O)$_{amide}$ and ν(C=N)$_{pyr}$ indicates the coordination mode and the number of coordination sites of piroxicam to a metal ion [33]. In the IR spectrum of *trans*-[Ru(Pir)$_2$(CH$_3$CN)$_2$], two absorptions at 1630 (ν(C=O)$_{amide}$) and 1575 cm^{-1} (ν(C=N)$_{pyr}$) are shifted to 1622.8 and 1571.7 cm^{-1}, respectively, and these shifts confirm the coordination of Pir$^-$ to the Ru(II) ion through the pyridyl nitrogen and the amide oxygen atoms. The sharp absorption band attributed

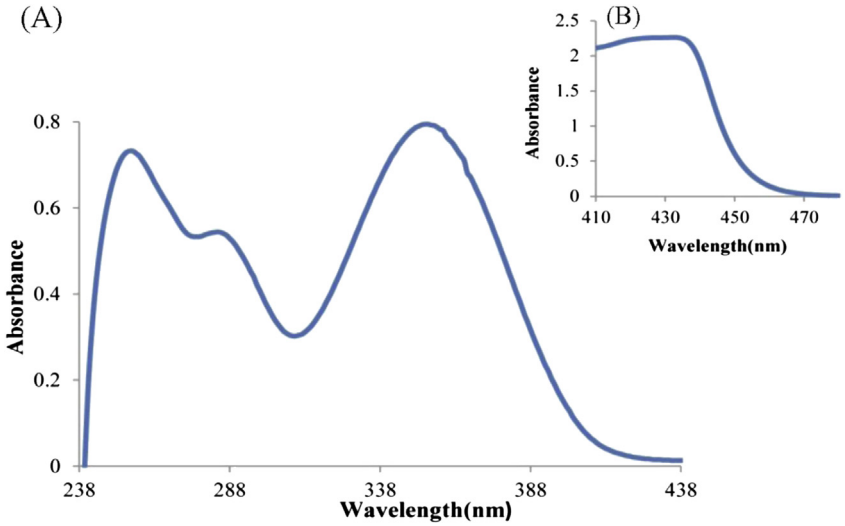

Fig. 2. Electronic spectra of the Pir^- anion; (A) 2.5×10^{-5} M (B) 2×10^{-2} M in acetonitrile at room temperature.

to the N–H stretching vibration of the Pir^- anion changes to a broad peak in the IR spectrum of complex due to the presence of a strong intramolecular hydrogen bonding between the $(N–H)_{amide}$ and $(O^-)_{enolate}$ atoms of the piroxicam ligands in the Ru(II) complex. The SO_2 antisymmetric and symmetric stretching vibrations located at 1352 and 1182 cm^{-1}, respectively, are almost unchanged with respect to the free ligands. This observation provides evidence that the SO_2 functional group is not involved in the coordination to Ru(II). The electronic spectra in the ultraviolet and visible ranges for the uncoordinated Pir^- anion (Fig. 2) and *trans*-$[Ru(Pir)_2(CH_3CN)_2]$ (Fig. 3) were recorded in acetonitrile solution. The spectrum of Pir^- displays a band at 256 nm which is attributed to an $n \rightarrow \pi^*$ transition of the amide C=O group. Upon complexation, this band is blue-shifted to 246 nm. The band at 354 nm which is assigned to $n \rightarrow \pi^*$ transition band of the pyridyl nitrogen atom in the free Pir^- anion is red-shifted to 378 nm upon complexation. These changes confirm the donation of the lone pair electrons of the O_{amide} and N_{pyr} atoms to Ru(II) [33].

3.3. DNA-binding properties

3.3.1. Electronic absorption titration

The interactions of the Pir^- anion and the Ru(II) complex with DNA were investigated by the UV–Vis absorption titrations. The UV–Vis absorption spectra of the Pir^- anion and the Ru(II) complex were significantly affected by the addition of increasing amounts of DNA. The absorption band of Pir^- at 255 nm was red-shifted by ca. 2 nm and its intensity was lowered on the addition of DNA up to stoichiometric ratio [DNA]/[drug] = 1.0 while there was an increase in the absorption intensity at higher molar ratios (Fig. 4A). All these findings support the hypothesis of DNA intercalating interactions of Pir^- through the stacking interaction of the aromatic rings of the ligand and the base pairs of DNA [34]. The absorption band of the Ru(II) complex at 246 nm is red-shifted by about 8 nm and shows hyperchromism of about 60% upon addition of DNA (Fig. 5A). These spectral changes are as a result of a complex bound to DNA through groove binding mode and have been observed in case of some

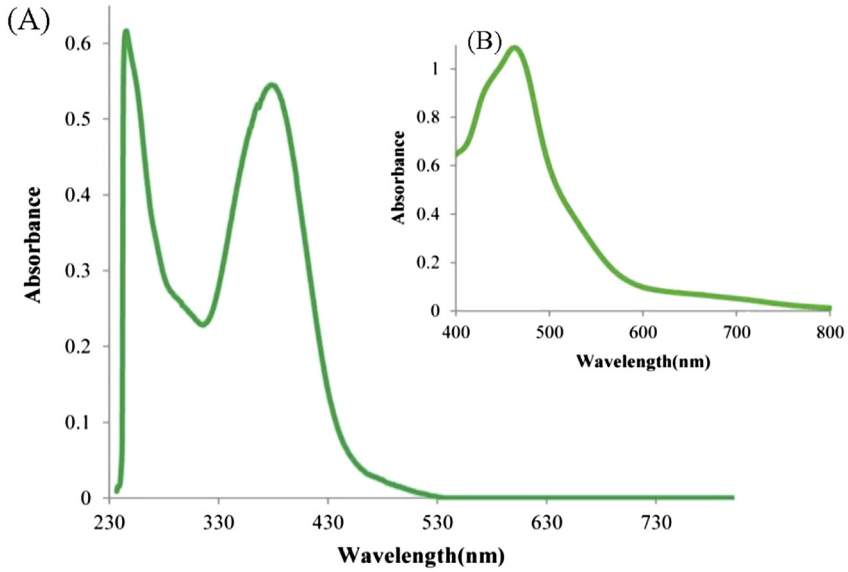

Fig. 3. Electronic spectra of the Ru(II) complex; (A) 2.5×10^{-5} M (B) 2×10^{-2} M in acetonitrile at room temperature.

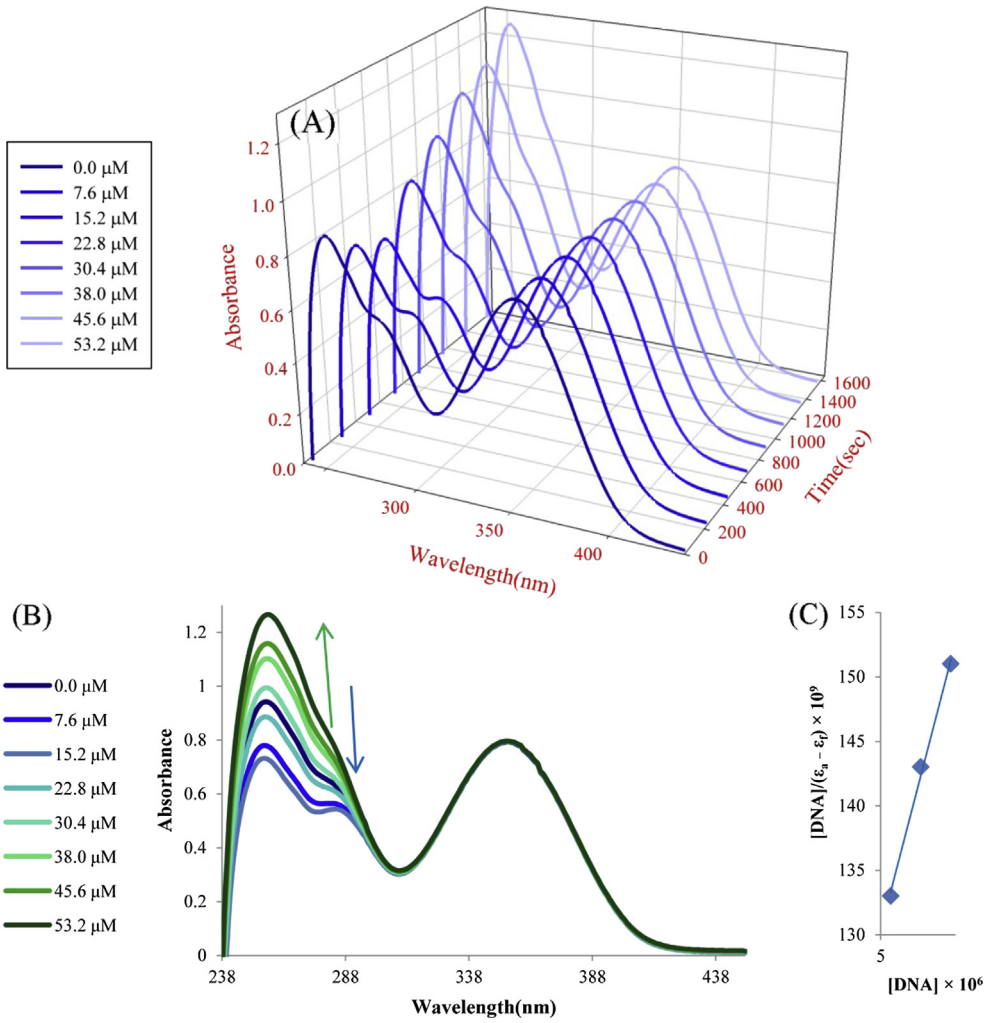

Fig. 4. (A) Three dimensional graph showing changes in the wavelength, absorbance and time. (B) Absorption spectra of the Pir^- anion (35 μM) in buffer solution (5 mM Tris–HCl/10 mM NaCl at pH 7.2) in the presence of increasing amounts of FS-DNA (0–53.2 μM) in 0.7% aqueous DMSO at 25 °C. Arrows show the intensity changes upon increasing the DNA concentration (C) Plots of [DNA]/($\varepsilon_a - \varepsilon_f$) versus [DNA] for the titration of the Pir^- anion with FS-DNA.

complexes upon their interaction with DNA [35,36]. The "hyperchromic effect" was due to the dissociation of ligand aggregates or due to its external contact (surface binding) with the duplex by engaging in hydrogen bonding interactions between the coordinated NH and OH groups with the functional groups positioned on the edge of DNA bases [37].

To quantitatively compare the DNA-binging strengths of the free Pir^- anion and the Ru(II) complex, their intrinsic binding constants, K_b, were determined by monitoring the changes in the absorbance at 255 nm for the Pir^- anion and at 246 nm for the Ru(II) complex, with increasing concentration of DNA, and by using Eq. (1) [38]:

$$\frac{[DNA]}{(\varepsilon_a - \varepsilon_f)} = \frac{[DNA]}{(\varepsilon_b - \varepsilon_f)} + \frac{1}{K_b(\varepsilon_b - \varepsilon_f)} \quad (1)$$

Where, [DNA] is the concentration of FS-DNA in base pairs, ε_a, ε_f and ε_b correspond to A_{obsd}/[complex], the extinction coefficient for the free Ru(II) complex and the extinction coefficient for the Ru(II) complex in the fully bound form, respectively, and K_b is the equilibrium binding constant in M^{-1}. In the plots of [DNA]/($\varepsilon_a - \varepsilon_f$) versus [DNA], K_b is given by the ratio of the slope to the intercept. Thus, the intrinsic binding constants (K_b) of the Pir^- anion (Fig. 4C) and the Ru(II) complex (Fig. 5C) were determined as 1.2×10^4 and 1.5×10^4 M^{-1}, respectively. The Ru(II) complex has higher affinity toward DNA, compared to the Pir^- anion which due to the presence of a Ru(II) cation in complex. The cation provides an enhanced interaction to the anionic DNA phosphate backbone and facilitates its binding to DNA.

3.3.2. Fluorescence quenching and competitive binding

Luminescence spectroscopy is one of the most sensitive ways to analyze drug interactions with biomolecules such as DNA and protein. After having studied the interaction of the Pir^- anion and the Ru(II) complex with DNA, it was observed that the Pir^- anion showed no significant changes in the emission spectra in the presence of increasing amounts of FS-DNA. The steady-state competitive binding experiment using the Pir^- anion as a quencher may give further information about the binding of the Pir^- to DNA. Ethidium bromide (3,8-diamino-5-ethyl-6-phenyl phenanthridinium bromide, EthBr) is a conjugate planar intercalating molecule and has an intense fluorescence in the presence of DNA, due to its strong intercalation between adjacent DNA base pairs [39]. Addition of the Pir^- stock solution to DNA pretreated with EthBr and then measurement of the emission intensities of DNA-bound EthBr, resulted in the reduction of emission intensity

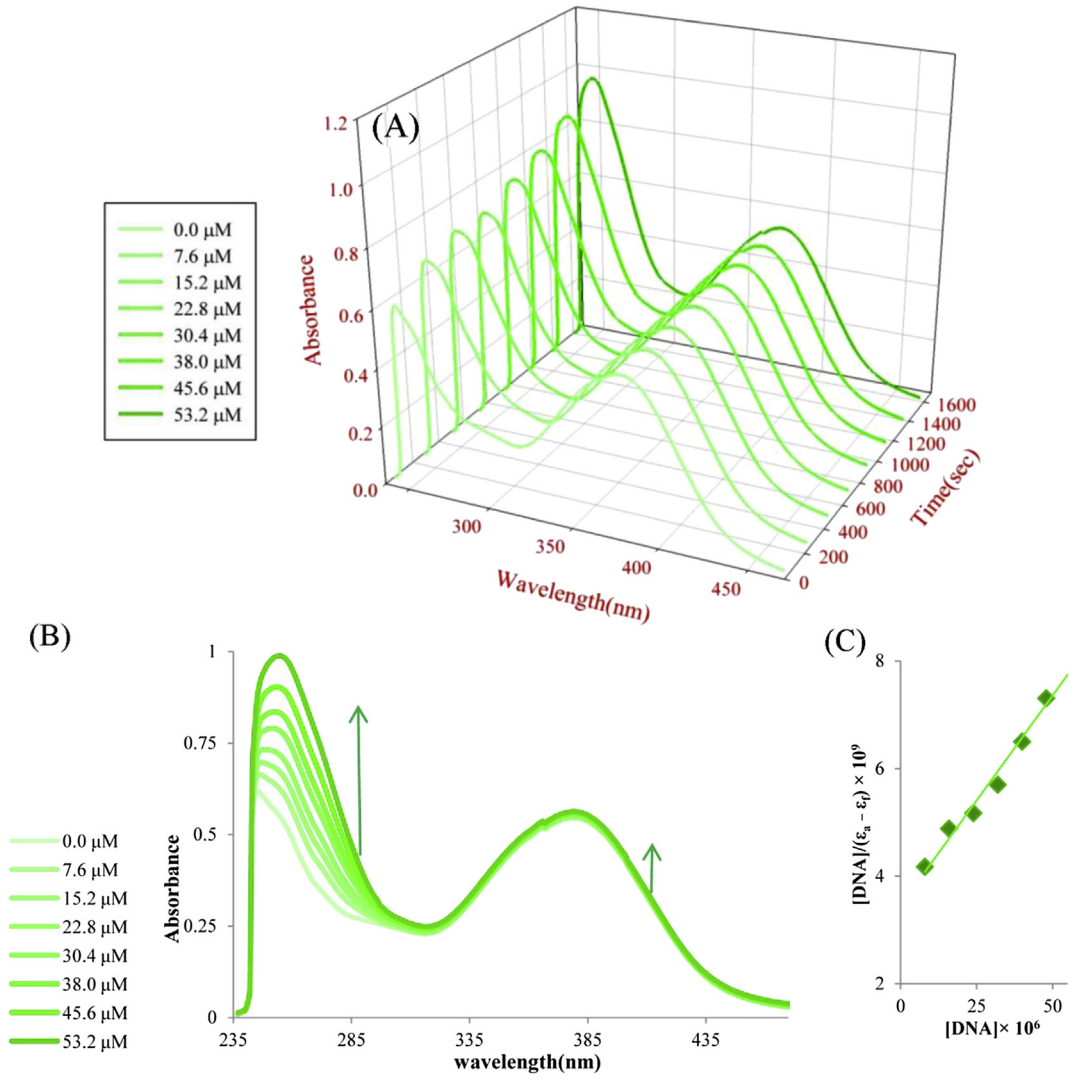

Fig. 5. (A) Three dimensional graph showing changes in the wavelength, absorbance and time. (B) Effect of the DNA concentration on the UV spectra of the Ru(II) complex (25 μM) in buffer solution (5 mM Tris–HCl/10 mM NaCl at pH 7.2) in the presence of increasing amounts of FS-DNA (0–53.2 μM) in 0.7% aqueous DMSO at 25 °C. Arrows show the intensity changes upon increasing the DNA concentration. (C) Plots of [DNA]/($\varepsilon_a - \varepsilon_f$) versus [DNA] for the titration of the Ru(II) complex with FS-DNA.

(Fig. 6A). The decrease in the emission intensity results when a second DNA binding molecule either replaces EthBr or accepts the excited electron from EthBr [40].

A competitive binding of Pir^- to the DNA would result in the displacement of the bound EthBr, leading to a reduction in the emission intensity due to the fluorescence quenching of the free EthBr molecules in an aqueous medium [41,42]. Therefore, the extent of quenching of fluorescence intensity of the EthBr molecule bound to DNA can be used to determine the binding ability between the Pir^- anion and DNA. Fluorescence quenching in terms of the quenching constant was determined following the Stern–Volmer Eq. (2) [43]:

$$\frac{I_0}{I} = 1 + K_{sv}[Q] \quad (2)$$

where, I_0 and I are the fluorescence intensities in the absence and presence of the quencher, respectively, K_{sv} is the Stern–Volmer quenching constant, and [Q] is the quencher concentration. The fluorescence data plotted as I_0/I versus the Pir^- concentration reveal the quenching constant, K_{sv}, as 1.13×10^4 M^{-1} for the interaction of Pir^- with DNA (Fig. 6B).

The Ru(II) complex emits luminescence in the Tris–HCl/NaCl buffer at 298 K, with a maximum at 351 nm. Upon addition of increasing amounts of FS-DNA (0–12 μM) to a fixed concentration of the Ru(II) complex (25 μM), the emission intensity decreases steadily (Fig. 7A). By plotting the relative fluorescence intensity as a function of the DNA concentration (Fig. 7B), the fluorescence quenching constant (K_{sv}) value was obtained as 1.77×10^4 M^{-1}, indicating that this complex shows a high quenching efficiency and a significant degree of binding to DNA.

3.4. BSA-binding properties

3.4.1. UV absorption spectra of BSA in the presence of the Pir^- anion and the Ru(II) complex

UV absorption spectrum is a very simple and applicable technique to explore the structural changes of protein and to investigate the protein–ligand complex formation [44]. BSA has two main absorption bands: one strong absorption peak in the range of 208–240 nm, which is the skeleton absorption peak resulted from the $\pi \rightarrow \pi^*$ transition of the polypeptide backbone structure and one weak absorption peak at about 278 nm due to the aromatic amino acids (Trp, Tyr, and Phe) [45]. It is well known that the absorption of

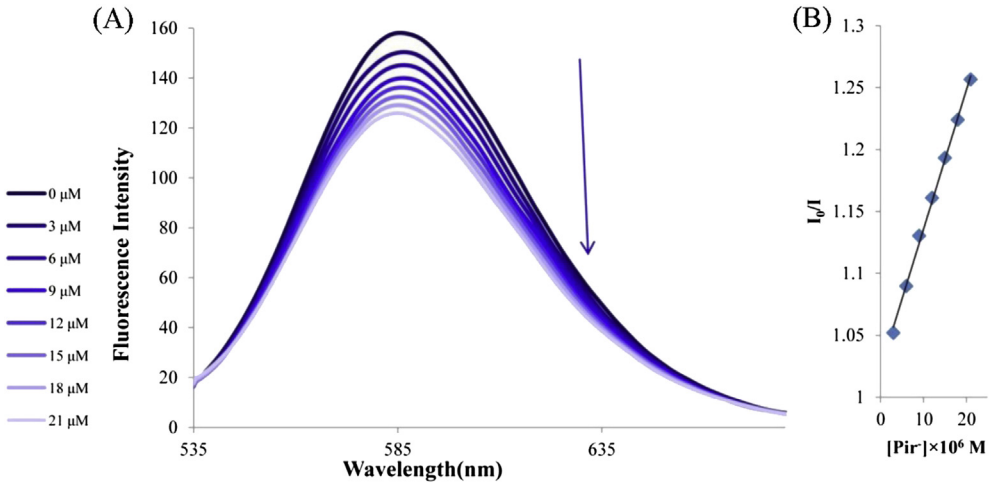

Fig. 6. (A) Emission spectra of EthBr bound to FS-DNA in the absence (0 μM) and presence of increasing amounts of the Pir^- anion (0–21 μM) at room temperature in Tris–HCl/NaCl buffer pH 7.2 (shown by arrow), [DNA] = 1.3×10^{-4} M, [Eth-Br] = 1.3×10^{-6} M, λ_{ex} = 520 nm. (B) Plot of I_0/I versus [Pir^-].

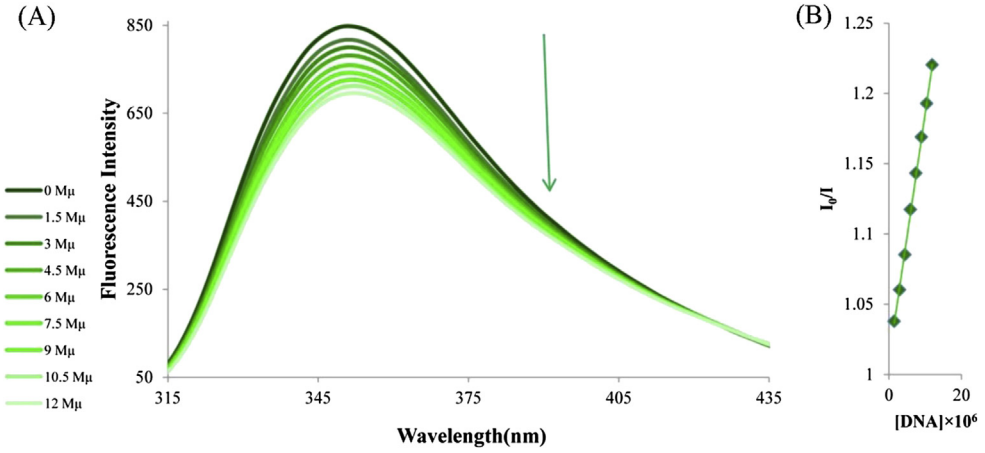

Fig. 7. (A) Emission spectra of the Ru(II) complex in Tris–HCl/NaCl buffer (pH 7.2) in the absence and presence of FS-DNA. Arrows show the intensity changes upon increasing the concentration of FS-DNA (0–12 μM). (B): Plot of I_0/I versus [DNA].

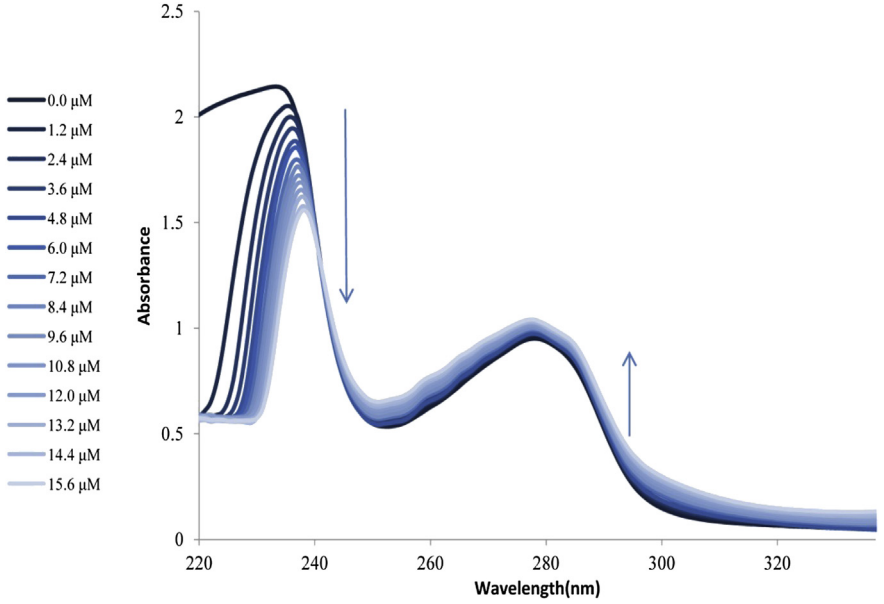

Fig. 8. (A) Absorption spectral traces of BSA in Tris–HCl/NaCl buffer upon addition of the Pir^- anion (0–15.6 μM). Arrow shows the intensity changes upon increasing the Pir^- concentration.

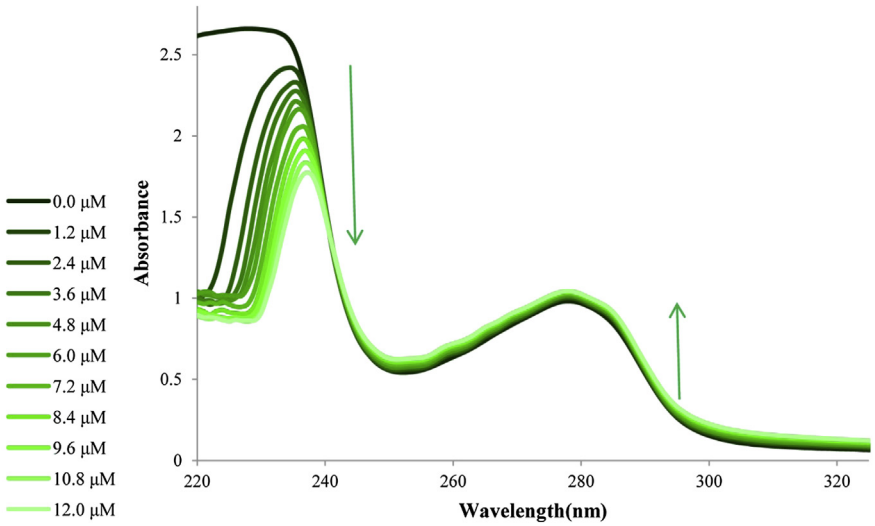

Fig. 9. (A) Absorption spectral traces of BSA in Tris–HCl/NaCl buffer upon addition of the Ru(II) complex (0–12 μM). Arrow shows the intensity changes upon increasing the concentration of Ru(II) complex.

a chromophore is changed in direction and magnitude that depends on whether it is transferred to a more hydrophobic or more hydrophilic environment. These shifts are ascribed to a change of $\pi \rightarrow \pi^*$ transition brought about by changes in the polarizability of the solvent [46]. By increasing the amounts of Pir^- added to the BSA solution, the intensity of the absorption peak of BSA at 228 nm obviously decreased, and the peak shifted slightly toward longer wavelength (from 228 to 238 nm), whereas the intensity of BSA peak at 278 nm increased, gradually accompanied by no significant shift in the maximum wavelength (Fig. 8). The absorption spectra of BSA showed the same changes in the presence of the Ru(II) complex (Fig. 9). These observations indicated that the interaction of the Pir^- anion and the Ru(II) complex with BSA may cause the conformational changes in BSA and change the polarity of the microenvironment around the tyrosine and tryptophan residues of BSA.

3.4.2. Tryptophan quenching experiment

Fluorescence spectroscopy is an effective method in detecting the conformational changes of proteins and the complex formation. The conformational changes of BSA were evaluated by the measurement of intrinsic fluorescence intensity of protein before and after addition of a quencher. The effect of the Pir^- anion and the Ru(II) complex on the BSA fluorescence intensity are shown in Figs. 10A and 11A, respectively. When different concentrations of the Pir^- anion and the Ru(II) complex were titrated into a fixed concentration of BSA, the fluorescence emission intensities of BSA at 344 nm gradually decreased, and with the further addition of drugs, the fluorescence intensity of systems decreased tardily in each titration curve which indicates the beginning of saturation of the BSA binding sites. These results showed that the interaction of the Pir^- anion and the Ru(II) complex with BSA could cause changes in the protein secondary structure leading to changes in the tryptophan environment of BSA [47].

In order to understand quantitatively the magnitude of the binding strength of the Pir^- anion and the Ru(II) complex with BSA, the linear Stern–Volmer equation is employed, Eq. (3) [48]:

$$\frac{I_0}{I} = 1 + K_{sv}[Q] = 1 + K_q\tau_0[Q] \quad (3)$$

where, I_0 and I represent the fluorescence intensities in the absence and presence of quencher, respectively, [Q] is the quencher concentration, K_{sv} is a linear Stern–Volmer quenching constant, K_q is the quenching rate constant of biomolecule, and τ_0 is the lifetime of the fluorophore in the absence of quencher with an average value of 10^{-8} s [49]. K_{sv} and K_q of the Pir^- anion and the Ru(II) complex can be obtained from the quenching plot slope of I_0/I versus [Q], (Figs. 10B and 11B, respectively). The K_q values for the Pir^- anion and the Ru(II) complex are 1.79×10^{12} M^{-1} s^{-1}($r = 0.9848$) and 9.98×10^{11} M^{-1} s^{-1}($r = 0.9902$), respectively. The maximum collision quenching constant of various kinds of quenchers to biopolymer is 2.0×10^{10} M^{-1} s^{-1} [43]. Obviously, the rate constants of protein quenching initiated by the Pir^- anion and the Ru(II) complex are greater than 2.0×10^{10} M^{-1} s^{-1}. These results show that the above quenching processes are not initiated by a dynamic collision but they are initiated by a static quenching process through the formation of a complex. Therefore, the quenching of the BSA fluorescence by the Pir^- anion and the Ru(II) complex depends on the formation of a complex between them and BSA. For a static quenching process, the Stern–Volmer quenching constant can be interpreted as the association constant or binding constant (K_b) because the static quenching process arises from the formation of the complex between the fluorophore and the quencher [50].

3.5. Binding constant and number of binding sites

The values of binding constant, K_b, and the number of binding sites per albumin or DNA molecule, n, can be determined by the slope and the intercept of the double logarithm regression curve of $\log[(I_0 - I)/I]$ versus $\log[Q]$ based on the Eq. (4) [51]

$$\log\frac{I_0 - I}{I} = \log K_b + n\log[Q] \quad (4)$$

The correlation coefficients larger than 0.9, indicates that the assumptions underlying the deviation of Eq. (4) are reasonable. The number of binding sites are 0.82 and 0.89 for the Pir^- anion (Fig. 12) and the Ru(II) complex (Fig. 13) on DNA, respectively. Also, the number of binding sites are 0.74 and 0.75 for the Pir^- anion (Fig. 14) and the Ru(II) complex (Fig. 15) on BSA, respectively, at the experimental condition. These results indicate that there are more binding sites on DNA than BSA for both drugs (Pir^- and *trans*-$[Ru(Pir)_2(CH_3CN)_2]$). The binding constants of both drugs with BSA and DNA follow this order: Ru(II) complex–DNA > Pir^-–DNA > Pir^-–BSA > Ru(II) complex–BSA.

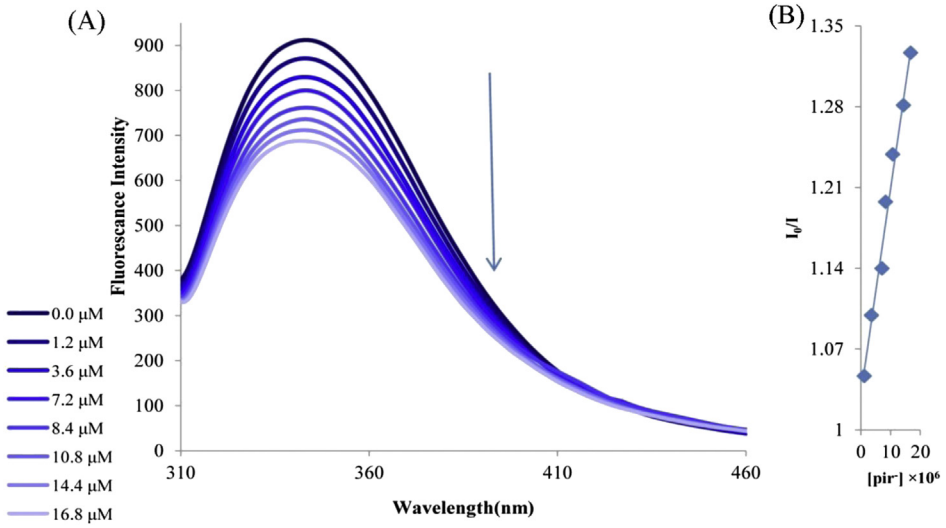

Fig. 10. (A) Fluorescence spectra of BSA (6×10^{-6} M) in the presence of different concentrations of the Pir^{-} anion (0–16.8 μM). (B) The Stern–Volmer plot for the fluorescence quenching of BSA by the Pir^{-} anion at 293 K.

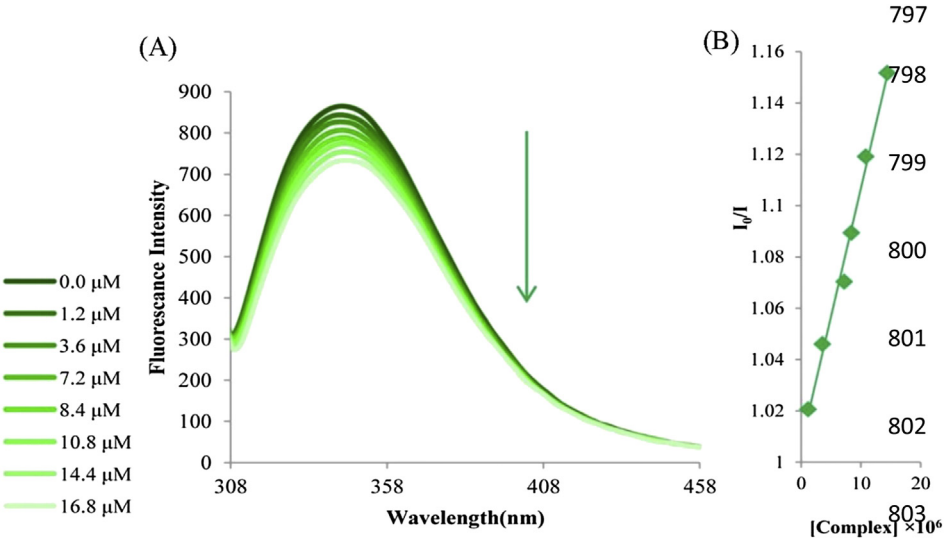

Fig. 11. (A) Fluorescence spectra of BSA (6×10^{-6} M) upon addition of different concentrations of the Ru(II) complex (0–16.8 μM). The arrow showed the increase in the concentration of complex. (B) The Stern–Volmer plots for the fluorescence quenching of BSA by the Ru(II) complex at 293 K.

3.6. Energy transfer between BSA and drugs

There are three types of intrinsic fluorophores in BSA, *viz.* tryptophan (Trp), tyrosine (Tyr), and phenylalanine (Phe) but the intrinsic fluorescence of BSA is mainly due to tryptophan. The importance of the energy transfer in biochemistry is that, the efficiency of transfer can be used to evaluate the distance, *r*, between the drug and the tryptophan residues in the protein. The energy transfer occurs under three conditions: (i) the presence of a fluorophore donor; (ii) a sufficient overlap between the fluorescence emission spectrum of the donor species and the UV–Vis spectrum of the acceptor species; (iii) the donor species is near to the acceptor (the distance less than 8 nm) [47]. According to Foster's non-radiative energy transfer theory (FRET), the rate of energy transfer depends on (i) the relative orientation of the donor and acceptor dipoles, (ii) the extent of overlap of fluorescence emission spectrum of the donor with the absorption spectrum of the acceptor and (iii) the distance between the donor and the acceptor [52]. The energy transfer effect is related not only to the distance between the acceptor and the donor, but also to the critical energy transfer distance, R_0, and the efficiency of energy transfer, *E*, which studied according to Forster's energy transfer theory. The value of *E* is calculated using Eq. (5) [52]:

$$E = \frac{I_0 - I}{I_0} = \frac{R_0^6}{r^6 + R_0^6} \tag{5}$$

where, *I* and I_0 are the fluorescence intensities of BSA in the presence and absence of quencher, *r* is the distance between acceptor and donor, and R_0 is the critical distance at which transfer efficiency equals 50%. R_0^6 can be calculated by the Eq. (6) [53]:

$$R_0^6 = 8.79 \times 10^{-25} K^2 N^{-4} \phi J \tag{6}$$

where, K^2 is the spatial orientation factor of the dipole for random orientations as in a fluid solution dependent on the alignment of

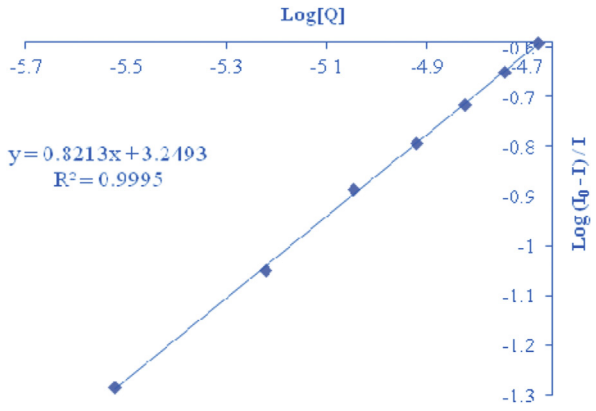

Fig. 12. Determination of the Pir^{-}-DNA binding constant and the number of binding sites on DNA at 298 K.

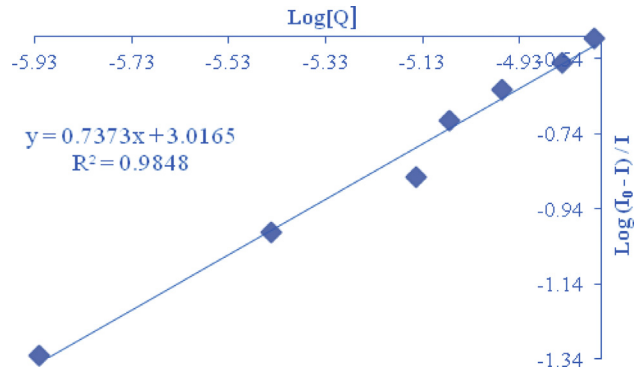

Fig. 14. Determination of the Pir^{-}-BSA binding constant and the number of binding sites on BSA at 298 K.

the donor and the acceptor dipoles, N is the refractive index of the medium, ϕ is the fluorescence quantum yield of the donor in the absence of the acceptor, and J is the overlap integral between the fluorescence emission spectrum of the donor and the absorption spectrum of the acceptor. J can be given by the Eq. (7) [54]:

$$J = \frac{\sum F(\lambda)\varepsilon(\lambda)\lambda^4\Delta\lambda}{\sum F(\lambda)\Delta\lambda} \quad (7)$$

where, $F(\lambda)$ is the fluorescence intensity of the donor at wavelength λ and $\varepsilon(\lambda)$ is the molar absorption coefficient of the acceptor at wavelength λ. For drug–BSA interaction, $K^2 = 2/3$, $N = 1.336$ and $\phi = 0.15$ [55]. According to the Eqs. (5)–(7), the values of the parameters for Pir^{-} were $J = 6.42 \times 10^{-20}$ cm^3Lmol^{-1} (Fig. 16), $R_0 = 3.478$ nm, $E = 0.193$ and $r = 4.416$ nm. The same parameters were calculated for the Ru(II) complex as $J = 1.75 \times 10^{-19}$ cm^3 L mol^{-1} (Fig. 17), $R_0 = 4.11$ nm, $E = 0.104$, and $r = 5.886$ nm. Obviously, the donor–acceptor distance is less than 8 nm, and $0.5R_0 < r < 1.5R_0$, implying that the energy transfer from BSA to the Pir^{-} anion and the Ru(II) complex occurs with high probability [56]. The bigger r value compared with that of R_0 again indicates the presence of a static quenching mechanism in the binding of Pir^{-} and the Ru(II) complex to BSA [57].

3.7. DNA photocleavage activity

There has been considerable interest in DNA endonucleolytic photocleavage reactions that are activated by the Ru(II) complexes [58,59]. The delivery of high concentrations of metal complex to the helix, in locally generating oxygen ($O^{\bullet}$) or hydroxide ($^{\bullet}OH$) radicals, yields an efficient DNA cleavage reaction [58].

Considering the above issue, the DNA photocleavage efficiency of the Pir^{-} anion and the Ru(II) complex were followed by monitoring the conversion of supercoiled (form I) DNA to the nicked circular (form II) or linear circular form (form III) species. The photocleavage patterns as a consequence of increasing concentration of the Ru(II) complex showed conversion of supercoiled into the nicked circular form without conversion to linear circular form (Fig. 19). Thus, it indicated that the complex is involved in a single strand DNA cleavage [60]. No such a DNA cleavage was observed when the Ru(II) complex was absent (lane a) or incubation of the plasmid DNA with complex in the dark. The photocleavage efficiency of the Ru(II) complex reached maximum at the concentration of 100 μM. But an increase in the concentration of the Pir^{-} anion led to lower degradation of plasmid pUC57 DNA. It can be clearly found from Fig. 18 that the DNA cleavage activity for the Pir^{-} anion is lower than the Ru(II) complex, which is in agreement with the results obtained from the DNA interaction studies.

3.8. Molecular docking of the Ru(II) complex with DNA sequence d(ACCGACGTCGGT)2

Although it is common to use molecular docking studies to suggest the most acceptable mechanism of the complex interaction with DNA or BSA sequence, but there is only a report about the molecular docking of Ru(II) complexes [60,61]. According to experimental reports, the Ru(II) complexes can bind to DNA in

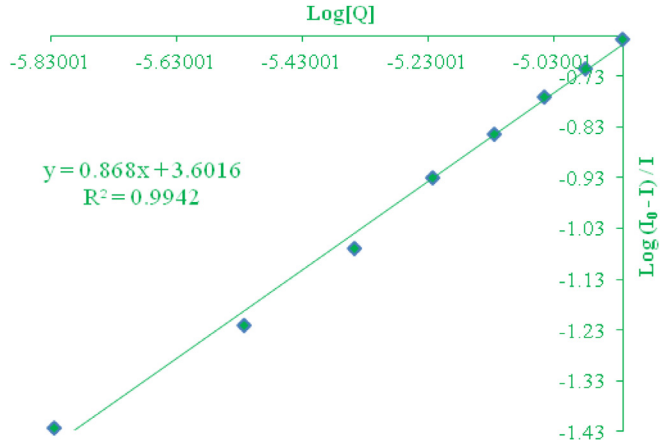

Fig. 13. Determination of the Ru(II) complex-DNA binding constant and the number of binding sites on DNA at 298 K.

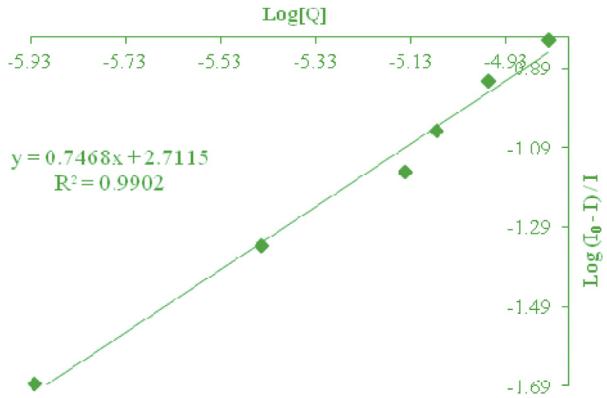

Fig. 15. Determination of the Ru(II) complex–BSA binding constant and the number of binding sites on BSA at 298 K.

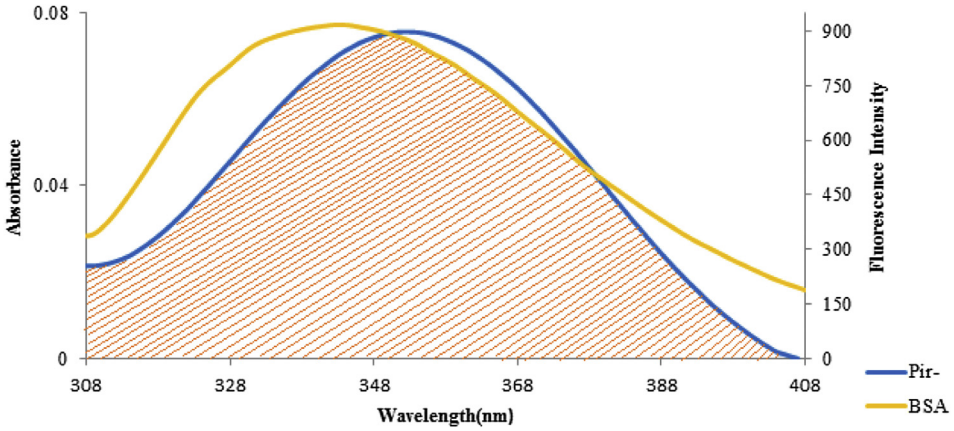

Fig. 16. Spectral overlap of the Pir^- absorption with the BSA fluorescence.

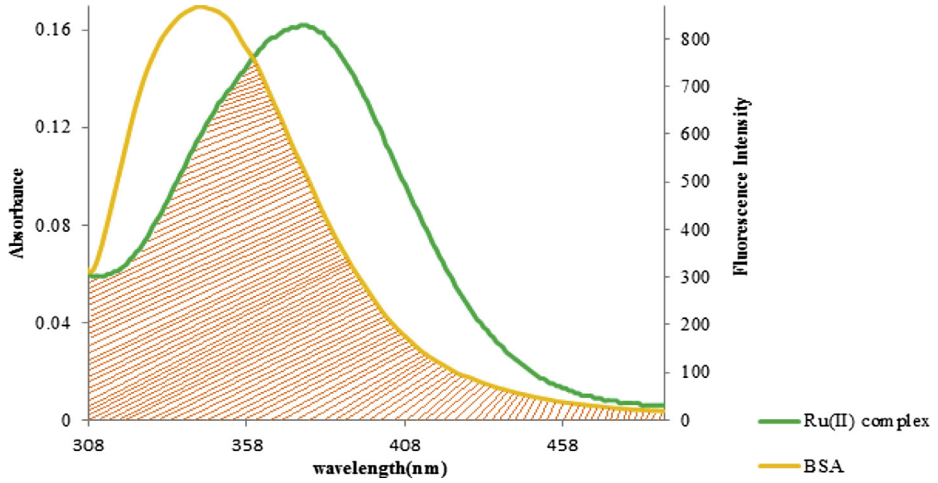

Fig. 17. Spectral overlap of the Ru(II)-complex absorption with the BSA fluorescence.

different interaction fashions such as groove binding, electrostatic binding, intercalative binding or partial intercalative binding [62–65].

The best conformer of DNA obtained from the MD simulation was docked with the Ru(II) complex. In order to generate of the metal complex coordinates, the X-ray crystal structure of the Ru(II) complex as a CIF file was converted to the PDB format by using the Mercury software (http://www.ccdc.cam.ac.uk/). The applied box size for docking was (74 × 58 × 58 Å) and grid spacing was 0.375 Å. The conformations were ranked based on the lowest binding free energy. The results of docking study revealed that the Ru(II) complex fitted into the DNA major groove. As shown in Fig. 20, there are hydrophobic contacts between C27, C28 and C29 with DC18, between C38 with DG16, C38 and S44 with DA17, and between C31 and C33 with DA5.

The minimum binding free energy of docked structure of the Ru(II) complex with DNA is −5.77 kcal mol^{-1} that indicates a good binding affinity between the Ru(II) complex and DNA.

3.9. Molecular docking study of the Ru (II) complex with BSA

The Ru(II) complex was docked with BSA conformer obtained from MD simulation. The blind docking on BSA showed that the Ru(II) complex prefers the binding pocket of domain I. The poses were ranked based on the lowest binding free energy. The Ru(II) complex is suited within the domain(I). As shown in Fig. 2, there are two hydrogen bonds between the Ru(II) complex and the BSA

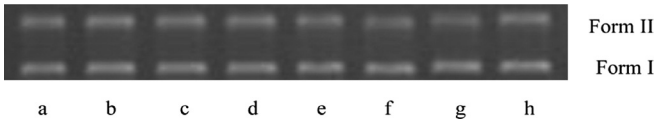

Fig. 18. Agarose gel electrophoresis diagram for the photocleavage pattern of pUC57 DNA (50 ng/μL) in the presence of different concentration of the Pir^- anion in Tris–HCl/NaCl buffer (pH = 7.2) upon irradiation by 360 nm light for 60 min after incubation at 37 °C for 1 h. Lane a: DNA control; Lane b: DNA + Pir^- (5 μM). Lane c: DNA + Pir^- (10 μM). Lane d: DNA + Pir^- (20 μM). Lane e: DNA + Pir^- (40 μM). Lane f: DNA + Pir^- (80 μM). Lane g: DNA + Pir^- (100 μM). Lane h: DNA + Pir^- (200 μM).

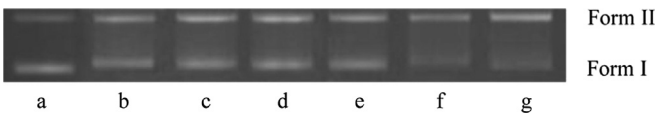

Fig. 19. Agarose gel electrophoresis diagram for the photocleavage pattern of pUC57 DNA (50 ng/μL) at different concentrations of the Ru(II) complex in Tris–HCl/NaCl buffer (pH = 7.2) upon irradiation by 360 nm light for 60 min after incubation at 37 °C for 1 h. Lane a: DNA control; Lane b: DNA + complex (5 μM). Lane c: DNA + complex (10 μM). Lane d: DNA + complex (20 μM). Lane e: DNA + complex (40 μM). Lane f: DNA + complex (80 μM). Lane g: DNA + complex (100 μM).

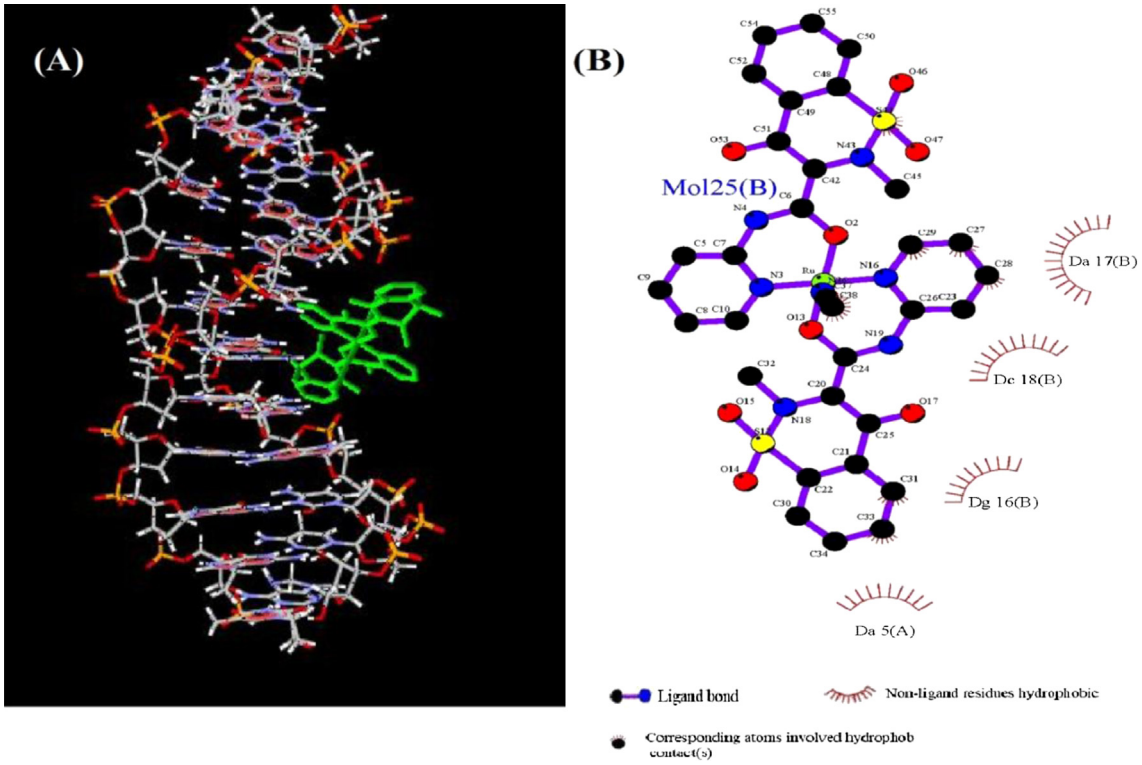

Fig. 20. (A) Molecular docking perspective of the Ru(II) complex with the major groove side of DNA using MVD. The complex depicted in a stick model, and DNA, represented in a wireframe model, (B) two-dimensional interactions generated by LIGPLOT.

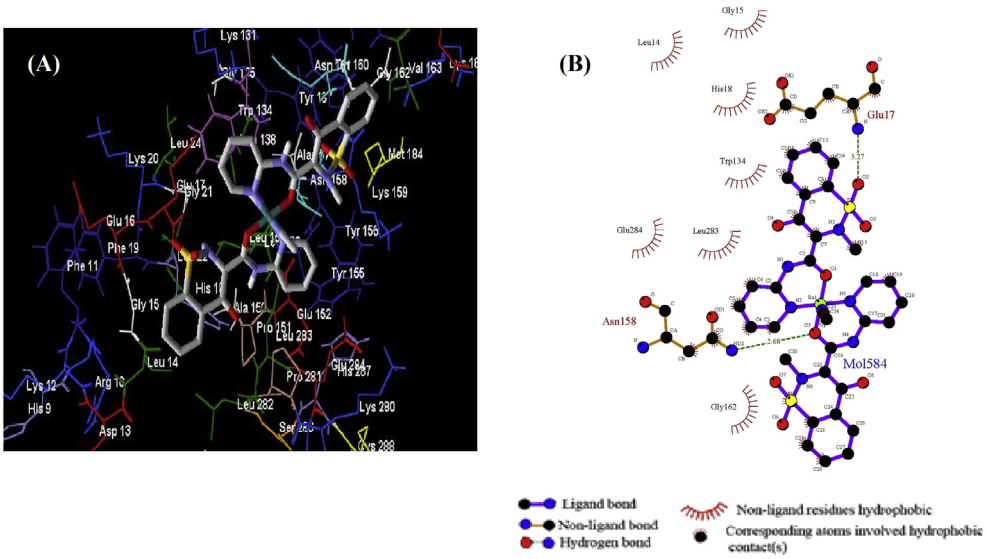

Fig. 21. (A) The docked Ru(II) complex in binding pocket of BSA using MVD. The complex depicted in a stick model, and BSA, represented in a wireframe model, (B) two-dimensional interactions generated by LIGPLOT.

amino acids. There are hydrogen bonding interactions between O_{SO2} with Glu17 (3.27 Å), and between O5 and Ans158 (2.68 Å). Also, there are hydrophobic contacts between C5, C6, C7, C8, C9, C10, C11, C13, C14, C15, C23, C28, C29 and C34 of the Ru(II) complex with Leu283, Glu284, Gly15, Leu14, His18, Trp134 and Gly162, as shown in Fig. 21.

The free energy change (ΔG^0) for binding of the Ru(II) complex with BSA found to be −5.21 kcal mol^{-1}.

4. Conclusion

In summary, a new mononuclear ruthenium(II) complex, *trans*-[Ru(Pir)$_2$(CH$_3$CN)$_2$], has been synthesized and fully characterized. Its DNA binding, BSA binding and photocleavage properties were also investigated. The spectroscopic studies show that the Pir$^-$ anion can intercalate into DNA base pairs because of its extended π system while the Ru(II) complex binds to DNA grooves. The

experimental results also show that the secondary structure of BSA molecules and the polarity of the microenvironment around the tyrosine and tryptophan residues change in the presence of the Pir^- anion and the Ru(II) complex. The binding distance between the donor (BSA) and the acceptors (Pir^- and *trans*-[$Ru(Pir)_2(CH_3CN)_2$]) were evaluated based on the Forster's theory of non–radiation energy transfer and the results indicated that the quenching of BSA by the Pir^- anion and the Ru(II) complex were static quenching processes. The photocleavage results of the plasmid pUC57 DNA show that the Ru(II) complex is more efficient DNA-photocleaver than the Pir^- anion. In addition, the binding of the Ru(II) complex to DNA and BSA were modeled by molecular docking and molecular dynamic simulation methods and the theoretical data confirm the experimental results with respect to the mechanism of binding and binding constants.

Acknowledgments

The financial support of the Research Council of the Isfahan University of Technology (IUT) is gratefully acknowledged. We are grateful to the Darou Pakhsh Pharmaceutical Company for providing us with the required piroxicam.

Appendix A. Supplementary data

CCDC 942718 contains the supplementary crystallographic data for this paper. These data can be obtained free of charge from The Director, CCDC, 12 Union Road, Cambridge CB2 1EZ, UK (fax: +44-1223-336033; e-mail: deposit@ccdc.cam.ac.uk or http://www.ccdc.cam.ac.uk). Electronic Supplementary Information (ESI) available: ^1H and ^{13}C NMR spectra for the piroxicam anion (Pir^-) and *trans*-[$Ru(Pir)_2(CH_3CN)_2$].

Appendix B. Supplementary data

Supplementary data related to this article can be found at http://dx.doi.org/10.1016/j.ejmech.2013.08.051.

References

[1] M. Galanski, M.A. Jakupec, B.K. Keppler, Curr. Med. Chem. 12 (2005) 2075–2094.
[2] I. Kostova, Recent Pat. Anticancer Drug Discov. 1 (2006) 1–22.
[3] G. Zhao, H. Lin, Curr. Med. Chem. Anticancer Agents 5 (2005) 137–147.
[4] F.P. Dwyer, E.C. Gyarfas, W.P. Rogers, J.H. Koch, Nature 170 (1952) 190–191.
[5] M.J. Clarke, in: H. Sigel (Ed.), Oncological Implications of the Chemistry of Ruthenium, Metal Ions in Biological Systems, M. Dekker, New York, 1980.
[6] C. Tan, J. Liu, H. Li, W. Zheng, S. Shi, L. Chen, L. Ji, J. Inorg. Biochem. 102 (2008) 347–358.
[7] G. Sava, A. Bergamo, S. Zorzet, B. Gava, C. Casarsa, M. Cocchietto, A. Furlani, V. Scarcia, B. Serli, B. Iengo, E. Alessio, G. Mestroni, Eur. J. Cancer 38 (2002) 427–435.
[8] A. Bergamo, R. Gagliardi, V. Scarcia, A. Furlani, E. Alessio, G. Mestroni, G. Sava, J. Pharmacol. Exp. Ther. 289 (1999) 559–564.
[9] C. Tan, J. Liu, L. Chen, S. Shi, L. Ji, J. Inorg. Biochem. 102 (2008) 1644–1653.
[10] G. Mestroni, E. Alessio, G. Sava, S. Pacor, M. Coluccia, A. Bocarelli, Met.-Based Drugs 1 (1993) 41–63.
[11] A. Kung, T. Pieper, R. Wissiack, E. Rosenberg, B.K. Keppler, J. Biol. Inorg. Chem. 6 (2001) 292–299.
[12] M. Ravera, S. Baracco, C. Cassino, P. Zanello, D. Osella, Dalton Trans. 7 (2004) 2347–2351.
[13] B.E. Bowler, K.J. Ahmed, W.I. Sundquist, L.S. Hollis, E.E. Whang, S.J. Lippard, J. Am. Chem. Soc. 111 (1989) 1299–1306.
[14] A. Bergamo, G. Sava, Dalton Trans. 13 (2007) 1267–1272.
[15] M.B. Sporn, N. Suh, Carcinogenesis 21 (2000) 525–530.
[16] (a) COSMO, Version 1.60, Bruker AXS Inc., Madison, Wisconsin, 2005; (b) SAINT, Version 7.06A, Bruker AXS Inc., Madison, Wisconsin, 2005; (c) SADABS, Version 2.10, Bruker AXS Inc., Madison, Wisconsin, 2005.
[17] M.C. Burla, R. Caliandro, M. Camalli, B. Carrozzini, G.L. Cascarano, L. De Caro, C. Giacovazzo, G. Polidori, R. Spagna, SIR2004, J. Appl. Cryst 38 (2005) 381–388.
[18] G.M. Sheldrick, SHELXL97, University of Gottingen, Gottingen, Germany, 1997.
[19] J. Marmur, J. Mol. Biol. 3 (1961) 208–218.
[20] K. Abdi, H. Hadadzadeh, M. Salimi, J. Simpson, A.A. Dehno Khalaji, Polyhedron 44 (2012) 101–112.
[21] G.M. Morris, D.S. Goodsell, R.S. Halliday, R. Huey, W.E. Hart, R.K. Belew, A.J. Olson, J. Comput. Chem. 19 (1998) 1639–1662.
[22] H. Park, J. Lee, S. Lee, Proteins: Struct. Funct. Bioinf. 65 (2006) 549–554.
[23] http://www.molegro.com/index.php of Comput. Chem. 25: 1605–1612, 2004.
[24] A.C. Wallace, R.A. Laskowski, J.M. Thornton, Protein Eng. 8 (1995) 127–134.
[25] D. Van der Spoel, E. Lindahl, B. Hess, G. Groenhof, A.E. Mark, H.J.C. Berendsen, J. Comput. Chem. 26 (2005) 1701–1718.
[26] V. Hornak, R. Abel, A. Okur, B. Strockbine, A. Roitberg, C. Simmerling, Struct. Funct. Bioinformat 65 (2006) 712–725.
[27] T. Darden, D. York, L. Pedersen, J. Chem. Phys. 98 (1993) 10089–10092.
[28] U. Essmann, L. Perera, M.L. Berkowitz, T. Darden, H. Lee, L.G. Pedersen, J. Chem. Phys. 103 (1995) 8577–8593.
[29] W.C. Swope, H.C. Andersen, P.H. Berens, K.R. Wilson, J. Chem. Phys. 76 (1982) 637–649.
[30] L. Rivail, C. Chipot, B. Maigret, I. Bestel, S. Sicsic, M. Tarek, J. Mol. Struct. 817 (2007) 19–26.
[31] H.J.C. Berendsen, J.P.M. Postma, W.F. Van Gunsteren, A. DiNola, J.R. Haak, J. Chem. Phys. 81 (1984) 3684–3690.
[32] K.F.D. Souza, J.A. Martins, F.B.T. Pessine, R. Custodio, Spectrochim. Acta Part A 75 (2010) 901–907.
[33] M.A. Zayed, F.A. Nour El-Dien, G.G. Mohamed, N.E.A. El-Gamel, Spectrochim. Acta Part A 60 (2004) 2843–2852.
[34] A. Silvestri, G. Barone, G. Ruisi, D. Anselmo, S. Riela, V.T. Liveri, J. Inorg. Biochem. 101 (2007) 841–848.
[35] I. Bhat, S. Tabassum, Spectrochim. Acta Part A 72 (2009) 1026–1033.
[36] P.M. Yang, L. Guo, B.S. Yang, Chin. Sci. Bull. 12 (1994) 987–989.
[37] R. Vijaylakashmi, M. Kanthimathi, V. Subramanain, B.U. Nair, Biochem. Biophys. Acta 1475 (2000) 157–162.
[38] H. Hadadzadeh, M. Salimi, M. Weil, Z. Jannesari, F. Darabi, K. Abdi, A.A. Dehno Khalaji, S. Sardari, R. Ahangari, J. Mol. Struct. 1022 (2012) 172–180.
[39] I. Haq, P. Lincoln, B. Norden, B.Z. Chowdhry, J.B. Chaires, J. Am. Chem. Soc. 117 (1995) 4788–4796.
[40] S. Mathur, S. Tabassum, Biometals 21 (2008) 299–310.
[41] A.M. Thomas, G. Neelakanta, S. Mahadevan, M. Nethaji, A.R. Chakravarty, Eur. J. Inorg. Chem. 76 (2002) 2720–2726.
[42] M. Lee, A.L. Rhodes, M.D. Wyatt, S. Forrow, J.A. Hartley, Biochemistry 32 (1993) 4237–4245.
[43] J.R. Lakowicz, G. Webber, Biochemistry 12 (1973) 4161–4170.
[44] Y.J. Hu, Y. Liu, J.B. Wang, X.H. Xiao, S.S. Qu, J. Pharm. Biomed. Anal. 36 (2004) 915–919.
[45] J.R. Lakowicz, G. Weber, Biochemistry 12 (1973) 1–61.
[46] M.G. Wen, X.B. Zhang, J.N. Tian, S.H. Ni, H.D. Bian, Y.L. Huang, H. Liang, J. Sol. Chem. 38 (2009) 391–401.
[47] N. Shahabadi, M. Mohammadpour, Spectrochim. Acta Part A 86 (2012) 191–195.
[48] M.R. Eftink, C.A. Ghiron, Anal. Biochem. 114 (1981) 199–227.
[49] J.R. Lakowicz, G. Weber, Biochemistry 12 (1973) 4171–4179.
[50] M. Durmus, V. Ahsen, J. Inorg. Biochem. 104 (2010) 297–309.
[51] M. Jiang, M.X. Xie, D. Zheng, Y. Liu, X.Y. Li, X. Chen, J. Mol. Struct. 692 (2004) 71–80.
[52] Y. Nia, S. Sub, S. Kokotc, Spectrochim. Acta Part A 75 (2010) 547–552.
[53] J.R. Lakowicz, Principles of Fluorescence Spectroscopy, third ed., Springer Science, New York, 2006.
[54] Y.Y. Yue, X.G. Chen, J. Qin, X.J. Yao, J. Pharm. Biomed. Anal. 49 (2009) 756–759.
[55] F. Ding, J.L. Huang, J. Lin, Z.Y. Li, F. Liu, Z.Q. Jiang, Dyes Pigm. 82 (2009) 65–70.
[56] Y.J. Hu, Y. Liu, L.X. Zhang, R.M. Zhao, S.S. Qu, Anal. Chem. 77 (2005) 1345–1353.
[57] W.Y. He, Y. Li, C.X. Xue, Z.D. Hu, X.G. Chen, F.L. Sheng, Bioorg. Med. Chem. 13 (2005) 1837–1845.
[58] K. Ashwini Kumar, K. Laxma Reddy, S. Vidhisha, S. Satyanarayana, Appl. Organometal. Chem. 23 (2009) 409–420.
[59] P. Kumar Yata, M. Shilpa, P. Nagababu, M. Rajender Reddy, L. Reddy Kotha, N.M.D. Gabra, S. Satyanarayana, J. Fluoresc 22 (2012) 835–847.
[60] R. Gaur, R. Ahmad Khan, S. Tabassum, P. Shah, M. Siddiqi, L. Mishra, J. Photochem, Photobiol. A: Chem. 220 (2011) 145–152.
[61] R. Ahmad Khan, A. Asim, R. Kakkar, D. Gupta, V. Bagchi, F. Arjmand, S. Tabassum, Organometallics 32 (2013) 2546–2551.
[62] G. Yang, L. Wang, L.N. Ji, J. Inorg. Biochem. 67 (1997) 289–290.
[63] G. Yang, J.Z. Wu, L. Wang, L.N. Ji, X. Tian, J. Inorg. Biochem. 66 (1997) 141–144.
[64] J.Z. Wu, L. Li, T.X. Zeng, L.N. Ji, J.Y. Zhou, R.H. Li, Polyhedron 16 (1997) 103–107.
[65] Y. Xiong, X.F. He, X.H. Zou, J.Z. Wu, X.M. Chen, L.N. Ji, R.H. Li, J.Y. Zhou, K.B. Yu, J. Chem. Soc. Dalton Trans. 23 (1999) 19–23.